Optical Materials: X 23 (2024) 100335

Contents lists available at ScienceDirect

Optical Materials: X

journal homepage: www.journals.elsevier.com/optical-materials-x

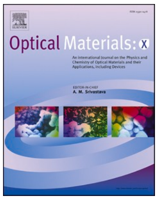

Highly efficient In(I) doped $Cs_3Cu_2I_5$ single crystals for light-emitting diodes and gamma spectroscopy applications

Xuemin Wen [a,b,1], Qiang Gao [a,b,1], Qian Wang [a], Weerapong Chewpraditkul [c], Mikhail Korjik [d], Shunsuke Kurosawa [e], Maksym Buryi [f], Vladimir Babin [g], Yuntao Wu [a,b,*]

[a] *Shanghai Institute of Ceramics, Chinese Academy of Sciences, 585 He-shuo Road, Shanghai, 201899, PR China*
[b] *Center of Materials Science and Optoelectronics Engineering, University of Chinese Academy of Sciences, Beijing, PR China*
[c] *Department of Physics, King Mongkut's University of Technology Thonburi, Thung-Khru, Bangkok, 10140, Thailand*
[d] *Institute for Nuclear Problems of Belarus State University, 11 Bobruiskaya, 220030, Minsk, Belarus*
[e] *NICHe, Tohoku University, 6-6-10 Aza-Aoba, Aramaki, Aoba-ku, Sendai, Miyagi, 980-8579, Japan*
[f] *Institute of Plasma Physics of the Czech Academy of Sciences, U Slovanky 2525/1a, 182 00, Prague, Czech Republic*
[g] *FZU - Institute of Physics of the Czech Academy of Sciences, 16200, Prague, Czech Republic*

ABSTRACT

High-quality $Cs_3Cu_2I_5$:In single crystals with a 7 mm diameter were grown by using the vertical Bridgman method. These crystals have a high optical transmittance (>75 %) and emit a bright red-orange light under both UV and X-ray irradiation. The $Cs_3Cu_2I_5$:In crystals can exhibit a high photoluminescence quantum efficiency (PLQY) of 79.5 %, thus we explored the potential applications for light-emitting diodes (LED). The fabricated LED demonstrated CIE color coordinates of (0.553, 0.431) with a color rendering index (Ra) of 77, making it suitable for supplementary light in plant growth. Moreover, we evaluated their gamma-ray spectroscopy capability by using an avalanche photodiode (APD) detector. Under ^{137}Cs gamma-ray irradiation, the gamma scintillation yield and energy resolution gradually degraded as the In concentration increased, which can be attributed to an enhanced afterglow after In doping.

1. Introduction

Single-component highly emissive halides are crucial for optoelectronic applications, including solid-state lighting, displays, fluorescent probes, and scintillators [1–5]. Low-dimensional lead-free halides have emerged as promising candidates owing to their eco-friendly characteristics, high PLQY, diverse polyhedral units, and tunable emission properties [6,7]. For instance, one-dimensional (1D) halides such as $CsCu_2I_3$, $Cs_5Cu_3Cl_6I_2$, Rb_2AgBr_3, and Rb_2CuBr_3, as well as zero-dimensional (0D) halides like $Cs_3Cu_2I_5$ and Cs_4EuBr_6, exhibit remarkable radioluminescence (RL) due to their strong quantum confinement effect arising from isolated metal-halide units at the molecular level [8–14]. $Cs_3Cu_2I_5$ has been identified as a highly promising component for scintillation applications owing to its excellent air stability, superior response to high-energy rays, and feasibility for large-scale growth [15–19]. Recently studies involving Mn^{2+}, Tl^+, and In^+ doping have significantly enhanced its scintillation yield, leading to improved X-ray or gamma-ray detection performances [20–26]. Besides, ^{6}Li doping expands its application scenarios to neutron−gamma discrimination [27]. Similarly to Tl^+ ions, In^+ doping to create scintillators has been under focus for decades. Nevertheless, oxide compounds having In ions to create matrices or doped with In ions demonstrated a light yield three times lower than $B_4Ge_3O_{12}$ (BGO) [28]. Notably, In-doped $Cs_3Cu_2I_5$ exhibits a bright red-orange emission and a high light yield (LY) of 53,000 photons MeV^{-1}, attributed to enhanced charge carriers harvesting efficiency in bulk $Cs_3Cu_2I_5$ single crystals [22]. This high scintillation yield, when combined with flexible paper, has enabled the achievement of a high X-ray imaging spatial resolution of 15 line pairs mm^{-1} for $Cs_3Cu_2I_5$:2%In^+@paper scintillation screen [23]. Additionally, Y. Tratsiak et al. conducted a detailed study on the luminescence properties of In^+ in $Cs_3Cu_2I_5$ elucidating the complex electronic structure and thermally-assisted radiative recombination processes from 12 to 300 K [29].

The red-orange broad-band emitting materials exhibit versatile applications across various fields [30,31]. Such light could stimulate the release of chlorophyll *a* and chlorophyll *b* in plant leaves, thereby enhancing the uptake of carbon dioxide and water, which in turn promotes plant growth and productivity [32]. Therefore, integrating red-orange luminescent materials with commercially available UV chips holds promise for fabricating phosphor-converted LEDs (pc-LEDs)

---

[*] Corresponding author. Shanghai Institute of Ceramics, Chinese Academy of sciences, 585 He-shuo Road, Shanghai, 201899, PR China.
E-mail address: ytwu@mail.sic.ac.cn (Y. Wu).

[1] Xuemin Wen and Qiang Gao both contributed equally to this work.

https://doi.org/10.1016/j.omx.2024.100335
Received 16 April 2024; Received in revised form 19 June 2024; Accepted 26 June 2024

tailored for plant supplementary lighting [32]. Moreover, in the realm of gamma-ray spectroscopy, this emission matches well with the detection spectral range of the high quantum efficiency (QE) avalanche photodiode (APD) detector (~98 %). Leveraging this high QE, one can anticipate a greater number of created electron-hole pairs [a number of photoelectrons in case of PMT], and exceptional energy resolution [33, 34]. To date, there has been a notable absence of specific reports regarding the applications of In^+-doped $Cs_3Cu_2I_5$ in LED and gamma-ray spectroscopy.

In this work, we synthesized high-quality $Cs_3Cu_2I_5$:x%In (in atomic ratio) crystals to explore their multifunctional applications in LED and gamma-ray detection. By coating the $Cs_3Cu_2I_5$:1%In powders on a 365 nm UV chip, the as-fabricated LED emits bright warm light with CIE color coordinates of (0.553, 0.431), which is in high demand for lighting. In doping enables the tunability of emission spectrum of $Cs_3Cu_2I_5$, spanning from blue to red-orange and into the near-infrared range, thereby enhancing compatibility with high QE APD detector. With increased In content, the corresponding emission-weighed quantum efficiency (EWQE) becomes improved from 79.4 % to 84.2 %. While the scintillation yield under X-ray irradiation raises up upon In concentration, the LY under gamma-ray irradiation continues to decrease. Additionally, the energy resolution gradually deteriorates with increasing In content. Finally, the afterglow measurement reveals the high afterglow level in $Cs_3Cu_2I_5$:In samples, which explains the above-mentioned LY reduction.

2. Experiment methods

2.1. Crystal growth

Single crystals of $Cs_3Cu_2I_5$ doped with varying In concentrations were grown by the vertical Bridgman method. High purity anhydrous CsI (99.999 %), CuI (99.999 %), and InI (99.999 %) beads were mixed according to the stoichiometric ratio, and then loaded into 7 mm diameter quartz ampules. The loaded ampules were dried at 120 °C under vacuum for 4 h to remove the residual moisture and oxygen. Subsequently, the ampules were sealed and transferred to a Bridgman growth furnace. With a temperature gradient of 22 °C cm^{-1} and a pulling rate of 0.4 mm h^{-1}, the ampules were translated from the top hot zone to the bottom cool zone. After the completion of the crystal growth process, the furnace was cooled to room temperature with a cooling rate of 10 °C h^{-1}.

2.2. Basic physical and optical characterization

Powder X-ray diffraction (PXRD) patterns were recorded using the $Cs_3Cu_2I_5$:In powders on a Bruker D8 VENTURE diffractometer (Cu Kα, $\lambda = 1.5418$ Å). Scanning electron microscopy (SEM) images, energy dispersive X-ray spectroscopy (EDS) elemental mapping, and the corresponding semiquantitative elemental analysis were measured using a Magellan 400 field-emission scanning electron microscopy. Optical transmission spectra of 2 mm thick $Cs_3Cu_2I_5$:In slabs within the range of 200–840 nm were recorded using an Agilent Cary 5000 UV–Vis–NIR spectrometer. PLQYs of $Cs_3Cu_2I_5$:In were measured by a Hamamatsu Photonics Quantaurus-QY Plus C13534-11 UV-NIR absolute PL quantum yield spectrometer, excited by a 150 W Xenon lamp. Photoluminescence excitation (PLE) and emission (PL) spectra were recorded on a Horiba FluoroMax + spectrofluorometer equipped with a steady-state Xenon lamp source. The PL decay kinetics profiles were measured using an Edinburgh Instruments FLS 980 spectrometer, excited by a pulsed nano-LED.

2.3. Fabrication and performance characterization of pc-LED

$Cs_3Cu_2I_5$:1 % In sample was manually ground to fine powders using the agate mortar. The powders were thoroughly mixed with epoxy resin (1:1 mass ratio) and coated on a 365 nm UV chip. Electroluminescence (EL) spectra were recorded using a Hopoo Optical & Electrical Fast Meters for LEDS. Image of the pc-LED in operation was captured using an iPhone 12 cellphone.

2.4. Scintillation performance characterization

Radioluminescence (RL) spectra of $Cs_3Cu_2I_5$:In and BGO slabs (4 x 4 × 2 mm^3) were measured using the combination of an OceanInsight QEpro High-performance CCD spectrometer and an X-ray generator (tungsten anode, operating voltage of 50 kV, operating current of 0.5 mA) within an integrating sphere. The X-ray-induced afterglow profiles were measured using the kinetic test module of the Horiba FluoroMax + spectrofluorometer with the above-mentioned X-ray generator. The ^{137}Cs gamma pulse height spectra (PHS) of $Cs_3Cu_2I_5$:In samples and BGO were acquired using the combination of the homemade High-performance Digital Spectrometer with a Hamamatsu S8664-1010 APD detector. The high voltage was set to 400 V, and the shaping time was set to 12.4 μs

3. Results and discussion

3.1. Physical properties of $Cs_3Cu_2I_5$:In single crystals

Ingots of $Cs_3Cu_2I_5$ and $Cs_3Cu_2I_5$:0.1 % In, each with a diameter of 7 mm, are shown in Fig. 1a. Under day light, 0 % In ingot appears colorless and transparent, while the 0.1 % In one shows slight coloring due to the In doping. Under UV light irradiation, 0 % In ingot emits blue light, whereas the 0.1 % one demonstrates a bright red-orange emission. As shown in Fig. 1b, $Cs_3Cu_2I_5$:In slabs with the size of 4 mm × 4 mm × 2 mm were polished for optical and scintillation characterizations. These slabs are transparent and free of inclusions. With the increase of In doping concentration, the slabs gradually change from colorless (0 % In sample) to faint yellow (2 % In sample). PXRD patterns of $Cs_3Cu_2I_5$:In are shown in Fig. 1c, matching well with the reflection peaks of the PDF card of $Cs_3Cu_2I_5$ (#97-015-0298), indicating the high phase purity of the $Cs_3Cu_2I_5$:In single crystals grown by the Bridgman method. The optical transmission spectra of 2 mm thick $Cs_3Cu_2I_5$: In slabs were recorded in Fig. 1d, with an overall transmittance of 75 %, indicating the high crystal quality of the slabs. The optical absorption edge shifts towards the longer wavelength as the In concentration increases, suggesting a significant narrowing of bandgap upon In doping, consistent with findings reported in the literature [35]. The EDS-based semiquantitative elemental analysis (Fig. 1e) of the $Cs_3Cu_2I_5$:1%In sample results in the following composition: Cs (28.71 %): Cu (19.95 %): I (51.34 %). It matches the stoichiometric ratio of $Cs_3Cu_2I_5$. In was not detected by EDS due to the low doping level (1 at%). Further, the EDS elemental mapping in Fig. 1f indicates the uniform distribution of Cs, Cu, and I in the $Cs_3Cu_2I_5$:1 % In sample.

3.2. Optical properties and pc-LED performance of $Cs_3Cu_2I_5$:In single crystals

To investigate the effect of In doping on the luminescence properties, the normalized PLE and PL spectra were measured and shown in Fig. 2a.

The In-free sample exhibits a broad PL emission peaking at 445 nm, attributed to the STE emission. Thus, a large Stokes shift of 141 nm (1.29 eV) was estimated based on the PLE of 304 nm (4.08 eV) and PL of 445 nm (2.79 eV). For the 0.3 % In sample, an additional emission in the range of 500–800 nm was observed. This emission centered at 624 nm was attributed to the In-related center [22,23,29]. It's noteworthy that In doping does not change the spectral shape of the PL and PLE of STE in this case. However, in the 2 % In sample, the PL peak position of STE emission shifts from 445 nm to 470 nm. As shown in Fig. 2a, since there is almost no overlap between the PL spectrum of the STE emission and the PLE spectrum of the In emission, there is negligible energy transfer

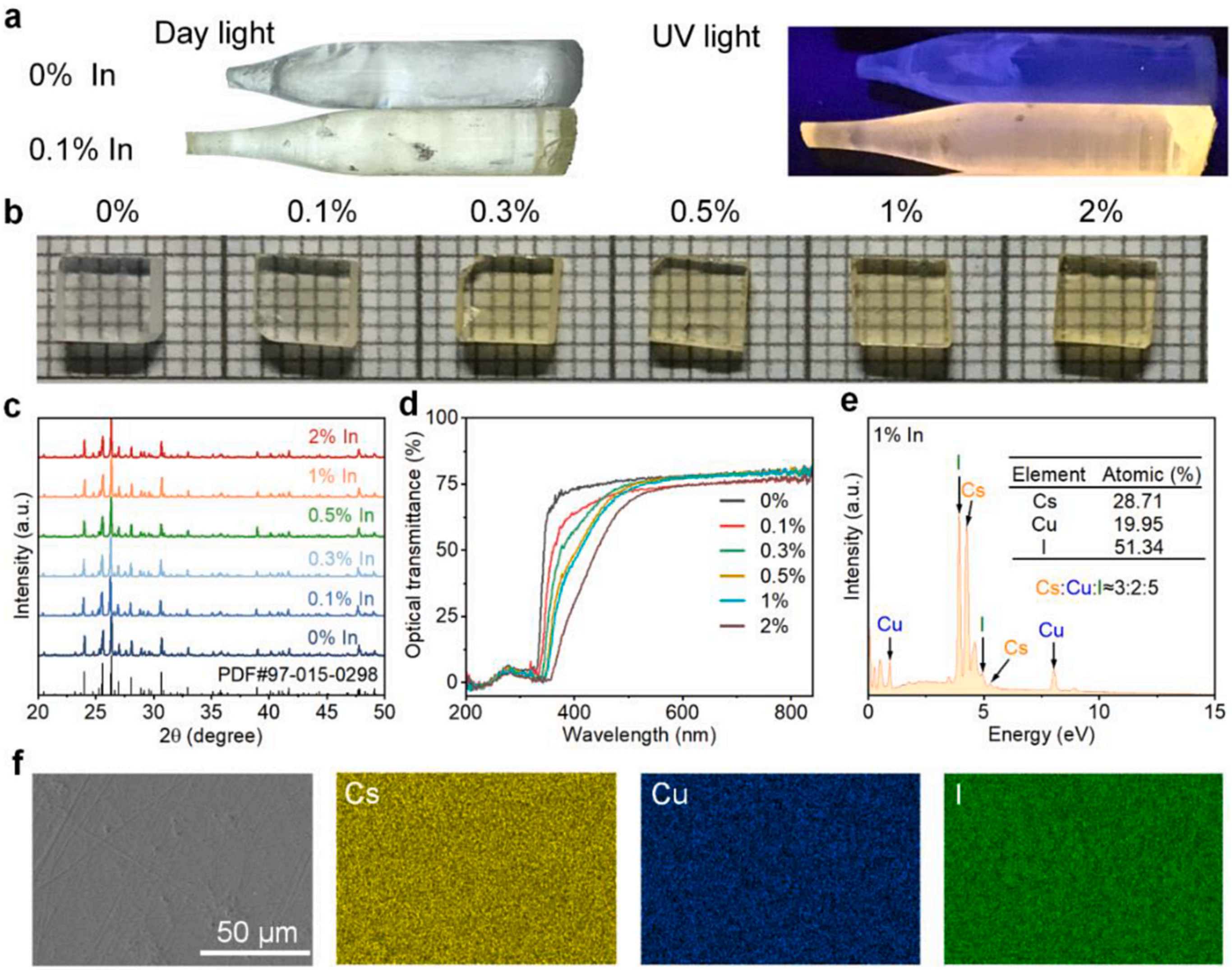

Fig. 1. (a) As-grown Ø 7 mm ingots of $Cs_3Cu_2I_5$ and $Cs_3Cu_2I_5$:0.1 % In under day light and UV light irradiation. (b) Polished $Cs_3Cu_2I_5$ crystal slabs doped with different In concentrations in the size of 4 mm × 4 mm × 2 mm under day light. (c) PXRD patterns of $Cs_3Cu_2I_5$:In samples. (d) Optical transmission spectra of 2 mm thick $Cs_3Cu_2I_5$:In slabs. (e) EDS survey spectra of $Cs_3Cu_2I_5$:1 % In slab. Inset table shows the atomic proportions analysis results. (f) EDS elemental mapping of $Cs_3Cu_2I_5$:1 % In slab.

between the two emission centers. Furthermore, the PL decay profiles of STE emission and In-related emission are shown in Fig. 2b and c, respectively. All the profiles could be well fitted by a single exponential function. The corresponding decay time values are shown in Fig. 2d as the functions of In content (0–2%). The decays of two centers are nearly unchanged, confirming that there is negligible energy transfer between the two centers. Furthermore, the corresponding PLQY of STE and In-related emissions were measured under excitation wavelengths of 304 nm and 340 nm, respectively (Fig. 2e). As the amount of In increases, the PLQY of STE drops from about 88 % at 0 %–75 % at 0.1 % followed by the increase to about 90 % in the 0.5–1% range of In content. The PLQY is dropped to below 85 % at the 2 % of In. The In-related emission exhibits much more pronounced and similar trend to the STE increasing from 25 % at the 0.1 % to about 79.5 % at the 1 % of In. The PLQY is dropped to below 70 % at 2 % of In. The trend of the PLQY when moving from 1 to 2 % of In is about the same for the STE and In-related emission. This observation could be attributed to the concentration quenching due to high In content doping. Detailed comparisons of the PLQY of $Cs_3Cu_2I_5$ reported in literature are summarized in the following Table 1.

Based on the observations above, the emission wavelength of $Cs_3Cu_2I_5$ under UV light irradiation can be easily tuned from the blue to the bright red-orange region by mixing STE and In-related emission in different proportion through the adjustment of the In doping level. This broad emission (550–800 nm) can be used for warm-color illumination and light supplementation [31,32]. Thus, $Cs_3Cu_2I_5$:In seems to be a potential candidate for single-component pc-LED. Therefore, we chose $Cs_3Cu_2I_5$:1%In sample for further experiments mainly considering that it possesses the highest PLQY of In-related emission (75.5 %, Fig. 2e). A mixture of $Cs_3Cu_2I_5$:1%In powders and epoxy resin were coated onto a 365 nm UV chip to fabricate the pc-LED. The corresponding EL spectrum under a 20 mA driven current and a 3 V driven voltage is depicted in Fig. 3a. This pc-LED exhibits color coordinates of (0.553, 0.431) with a Ra of 77. Inset shows the working state of the as-fabricated pc-LED, emitting bright warm light.

The printed pattern is clear and visible under the light. Current-dependent EL spectra are shown in Fig. 3 b, and no current saturation state is observed across the range of 20–100 mA. Fig. 3c shows the EL intensity at the peak position at 637 nm under different driven currents. The pc-LED reaches the maximum EL intensity at a driven current of 100 mA, after which the intensity decreases with the increasing driven current due to commonly known saturation effect. In conclusion, the

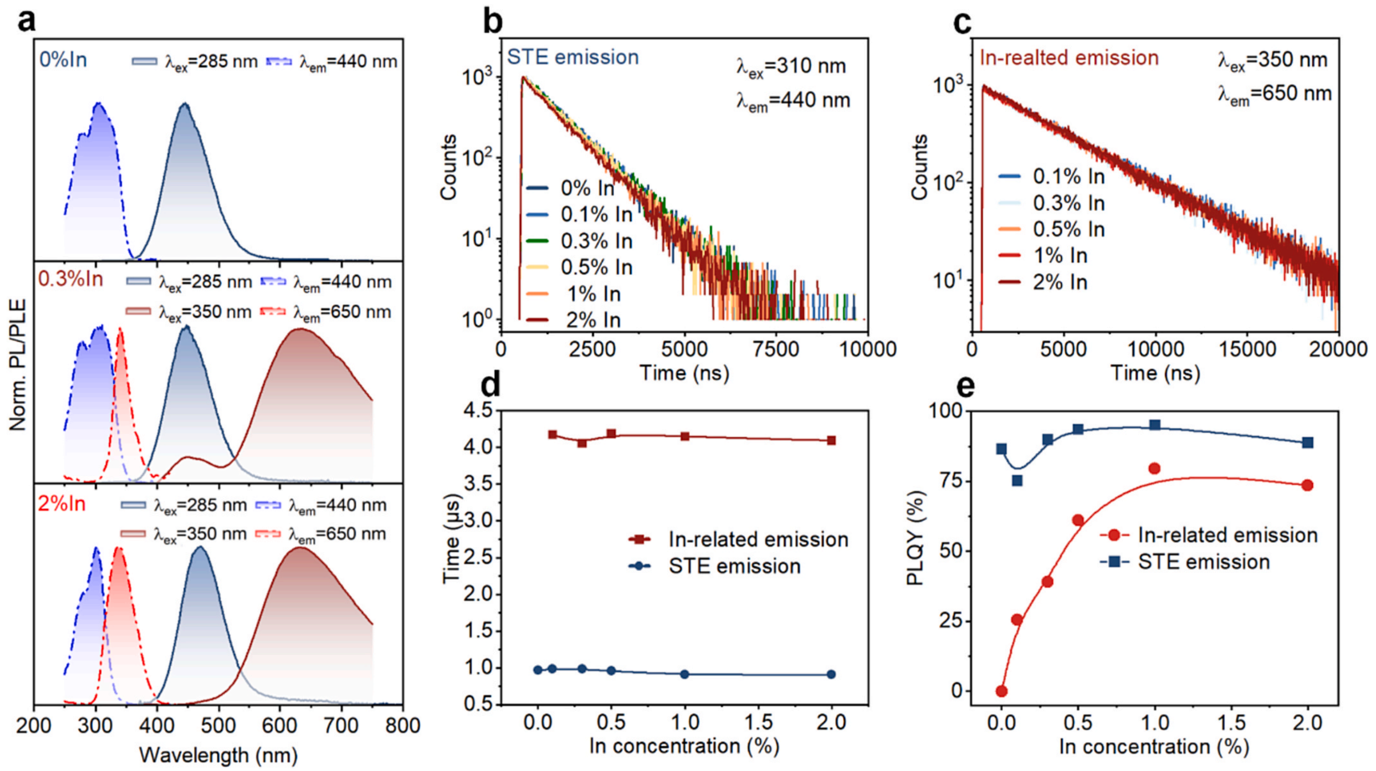

Fig. 2. (a) PL and PLE spectra of $Cs_3Cu_2I_5$ (top), $Cs_3Cu_2I_5$:0.3 % In (middle), and $Cs_3Cu_2I_5$:2 % In (bottom). PL decay profiles of STE emission (b) and In-related emission (c). (d) PL decays of STE emission and In-related emission as a function of In concentrations. (e) PLQY results of $Cs_3Cu_2I_5$:In samples as a function of In concentrations.

Table 1
Summary of PL emission performance of $Cs_3Cu_2I_5$.

Materials	Form	PL peak (nm)	PLQY (%)	Reference
$Cs_3Cu_2I_5$	NCs	445	47.19	[16]
$Cs_3Cu_2I_5$	NCs	440	96.6	[17]
$Cs_3Cu_2I_5$	SCs	445	97.76	[15]
$Cs_3Cu_2I_5$	SCs	455	93.5	[18]
$Cs_3Cu_2I_5$	SCs	445	69.9	[19]
$Cs_3Cu_2I_5$	SCs	445	88	This work
$Cs_3Cu_2I_5$:In	SCs	624	75	This work

$Cs_3Cu_2I_5$:In based pc-LED with the optimized power supply conditions (current of 100 mA and voltage of 3V) thus indeed has the application potential.

3.3. *Gamma spectroscopy performance of $Cs_3Cu_2I_5$:In single crystals*

RL spectra of $Cs_3Cu_2I_5$:In samples are shown in Fig. 4a as well as the BGO reference with identical size. The corresponding emission ratio of STE and In-related center to the total RL were estimated based on their integral spectral area using Gaussian fitting (Fig. 4b). The STE emission ratio sharply decreases to 11.6 % as the In doping concentration reaches 2 %. Meanwhile, with higher In content, the In-related emission ratio shows an increasing trend, reaching up to 88.4 % in the 2 % In sample.

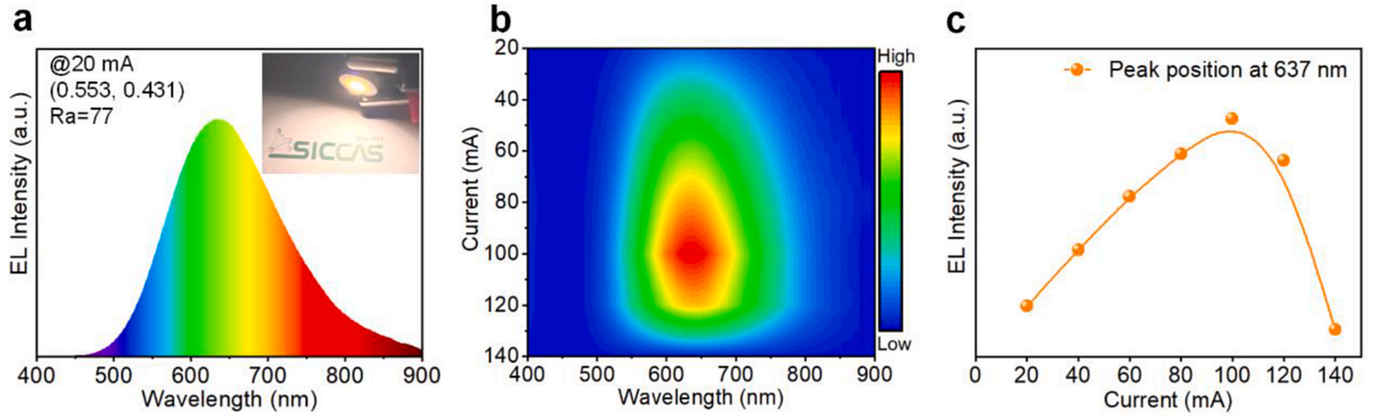

Fig. 3. (a) EL spectrum of as-fabricated pc-LED of $Cs_3Cu_2I_5$:1 % In by combining with a 365 UV chip. Inset shows the image of the working state of the warm-white pc-LED. (b) Current-dependent EL spectra contour mapping of the pc-LED of $Cs_3Cu_2I_5$:1 % In. (c) EL intensity of the peak position at 637 nm under different driven current.

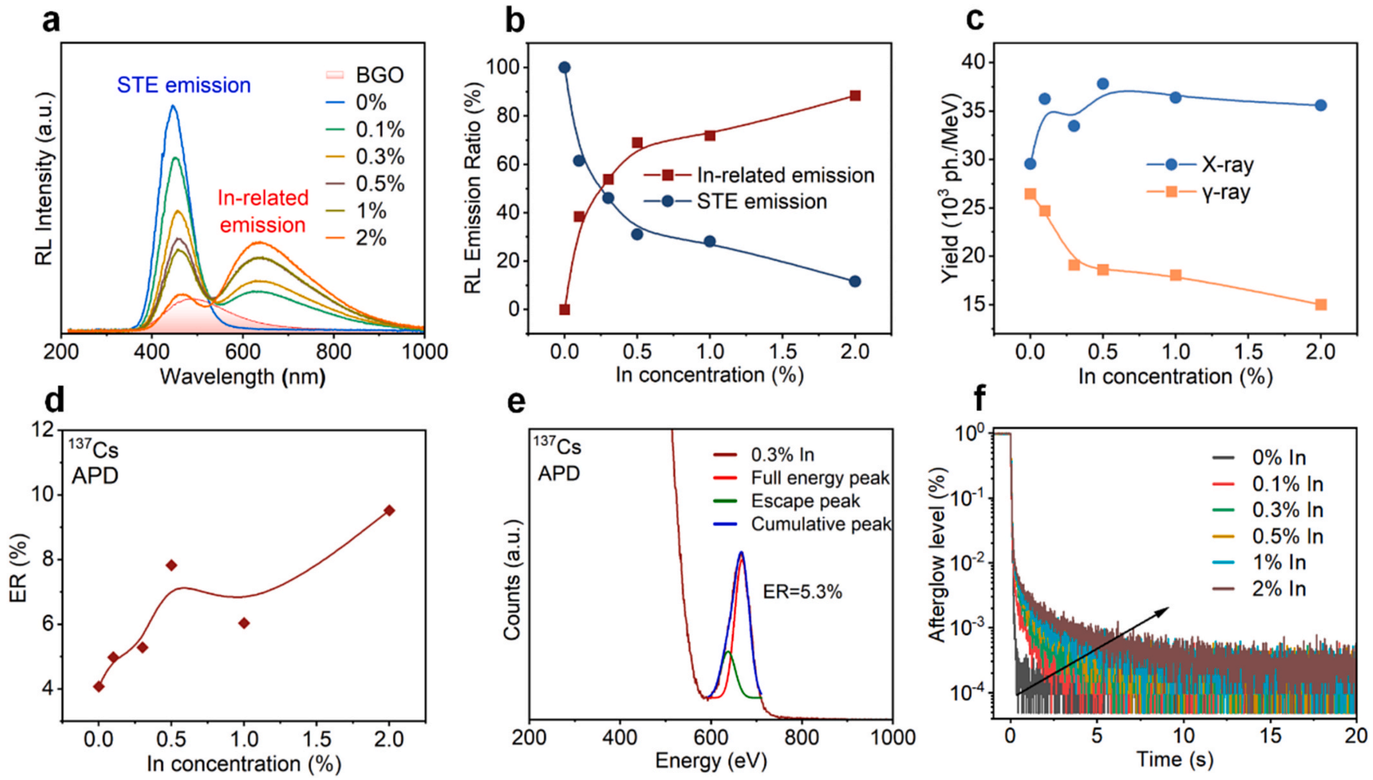

Fig. 4. (a) RL spectra of $Cs_3Cu_2I_5$:In and BGO slabs measured with the identical size of 4*4*2 mm^3 in an integrating sphere. (b) Ratio of STE and In-related emission to total RL emission as a function of In concentration. Yields (c), and ER (d) of $Cs_3Cu_2I_5$: In samples as a function of In concentration. (e) Representative PHS of $Cs_3Cu_2I_5$:0.3 % In measured with an APD under the ^{137}Cs gamma-ray irradiation. (f) Afterglow profiles of $Cs_3Cu_2I_5$:In samples.

This is in good agreement with PL above (Fig. 2). This indicates a strong competitive relationship between the two emission centers. In doping manipulates the emission rates of both STE and the In-related centers, thereby achieving the redshift of the RL spectra to better match the sensitive detection region of the high QE APD detector. The emission-weighed quantum efficiency (EWQE) of $Cs_3Cu_2I_5$:In samples were evaluated using the [34] following equation (1):

$$EWQE = \frac{\int_{\lambda_{min}}^{\lambda_{max}} RL(\lambda)QE(\lambda)d(\lambda)}{\int_{\lambda_{min}}^{\lambda_{max}} RL(\lambda)d(\lambda)} \tag{1}$$

Where RL(λ) is the normalized RL intensity at wavelength λ, and the QE(λ) is the QE of Hamamatsu S8664-1010 APD at wavelength λ here, λ_{min}-λ_{max} is the total interval region of the emission band. The extracted EWQE increases gradually from 79.4 % (0%In sample) to 84.2 % (2 % In sample), indicating that more electron-hole pairs (but more photoelectrons in case of PMT) will be created in the APD, thereby favoring an improved energy resolution. The steady-state scintillation yield (under X-ray irradiation) and LY (under γ ray excitation) of $Cs_3Cu_2I_5$:In slabs were evaluated based on the methods described in our previous works and summarized in Fig. 4c [5,33,34]. An increasing trend in steady-state scintillation yield is observed, which has been ascribed to the enhancement of harvesting efficiency of charge carriers produced in $Cs_3Cu_2I_5$ after In doping [22]. The steady-state scintillation efficiency reaches up to 37,800 photons MeV^{-1} when the In doping concentration is 0.5 at%. Subsequently, a decrease was observed to 35,600 photons MeV^{-1} in the 2 % In sample, mainly due to concentration quenching. This similar to the PLQY-related trends (Fig. 2e). At the same time, the obtained LY value (as measured within a short μs time gate, excluding delayed-radiative scintillation light) exhibits a continuous decrease from 26,500 photons MeV^{-1} for the In-free sample to 15,000 photons MeV^{-1} for the 2 % In sample. Consequently, the energy resolution deteriorates from 4.1 % for the In-free sample to 9.5 % for the 2 % In sample, as shown in Fig. 4d. The representative PHS of 0.3 % In sample is depicted in Fig. 4e, and an energy resolution of 5.3 % at 662 keV was estimated. Furthermore, we conducted the afterglow measurement for $Cs_3Cu_2I_5$:In samples. As shown in Fig. 4f, after X-ray irradiation cut-off, In doped samples exhibit more intense afterglow signals with the increase of In concentration, exceeding that of the In-free sample by more than one order of magnitude. Thus, the difference between the steady-state scintillation yield and the LY could be ascribed to the enhanced afterglow in doped samples. The energy of γ-ray is much larger than the energy of X-ray thus reaching the deep core levels and producing much more charges able to fill the traps existing in the material as compared to X-ray. Therefore, the afterglow is much more pronounced under the γ irradiation as compared to X-ray.

4. Conclusion

Bridgman-grown $Cs_3Cu_2I_5$:In single crystals emit a bright red-orange emission with a PLQY of 79.5 %. The intense EL emission from the fabricated pc-LED, with CIE color coordinates of (0.553, 0.431), demonstrates great potential of $Cs_3Cu_2I_5$:In supplementary light for plant growth. The LY and energy resolution, measured at 662 keV γ rays from a ^{137}Cs source, exhibit a gradual deterioration with increasing In content. Specifically, the LY decreases from 26,500 to 15,000 photons MeV^{-1}, while the energy resolution deteriorates from 4.1 % to 9.5 %. These observations were attributed to the enhanced afterglow level. Further efforts will be focused to improve the gamma spectroscopy capability of $Cs_3Cu_2I_5$:In crystals by suppressing afterglow intensity.

CRediT authorship contribution statement

Xuemin Wen: Writing – review & editing, Writing – original draft, Visualization, Validation, Software, Methodology, Formal analysis, Data curation. **Qiang Gao:** Writing – review & editing, Writing – original draft, Visualization, Validation, Methodology, Formal analysis, Data curation. **Qian Wang:** Visualization, Investigation. **Weerapong Chewpraditkul:** Writing – review & editing, Writing – original draft, Visualization, Validation, Supervision, Methodology, Investigation. **Mikhail Korjik:** Writing – review & editing, Writing – original draft, Visualization, Validation, Supervision, Methodology, Investigation. **Shunsuke Kurosawa:** Writing – review & editing, Writing – original draft, Visualization, Validation, Supervision, Methodology, Investigation. **Maksym Buryi:** Writing – review & editing, Writing – original draft, Visualization, Validation, Supervision, Software, Methodology, Investigation. **Vladimir Babin:** Writing – review & editing, Writing – original draft, Visualization, Validation, Supervision, Methodology, Data curation. **Yuntao Wu:** Writing – review & editing, Writing – original draft, Visualization, Validation, Supervision, Resources, Project administration, Methodology, Investigation, Funding acquisition, Formal analysis, Data curation, Conceptualization.

Declaration of competing interest

The authors declare that they have no known competing financial interests or personal relationships that could have appeared to influence the work reported in this paper.

Data availability

Data will be made available on request.

Acknowledgements

Thanks to Prof. Martin Nikl (FZU - Institute of Physics of the Czech Academy of Sciences, Czech Republic) for the discussion of this work. The financial support from the National Key R&D Program of China (2022YFB3503600), National Natural Science Foundation of China (11975303, 12211530561, 12305211), Shanghai Municipal Natural Science Foundation (21TS1400100), CAS Cooperative Research Project (121631KYSB20210017), CAS Project for Young Scientist in Basic Research (YSBR-024), project NSFC-23-11 of the National Natural Science Foundation of China (NSFC) and Czech Academy of Sciences is gratefully acknowledged.

References

[1] M. Zhang, P. Dang, Y. Wan, Y. Wang, Z. Zeng, D. Liu, Q. Zhang, G. Li, J. Lin, Adv. Opt. Mater. 12 (2024) 2302941.
[2] S. Wang, R. Liu, J. Li, F. Sun, Q. Yang, S. Li, J. Liu, J. Chen, P. Cheng, Adv. Sci. 10 (2023) 2303501.
[3] Y. Wang, T. Zhou, J. Chen, H. Qin, J. Wu, Q. Zhang, J. Zheng, X. Li, Y.Y. Sun, Y. He, X. Ma, T. Ye, R. Liu, Z. Gao, J. Hou, L. Wang, H. Chen, W. Jiang, Adv. Opt. Mater. 12 (2023) 2301864.
[4] J. Luo, X. Wang, S. Li, J. Liu, Y. Guo, G. Niu, L. Yao, Y. Fu, L. Gao, Q. Dong, C. Zhao, M. Leng, F. Ma, W. Liang, L. Wang, S. Jin, J. Han, L. Zhang, J. Etheridge, J. Wang, Y. Yan, E.H. Sargent, J. Tang, Nature 563 (2018) 541–545.
[5] X. Wen, Q. Wang, W. Li, Y. Li, S. Cheng, J. Wang, S. Kurosawa, Y. Wu, Phys. Status Solidi Rapid Res. Lett. 17 (2022) 2200341.
[6] J. Huang, T. Lei, M. Siron, Y. Zhang, S. Yu, F. Seeler, A. Dehestani, L.N. Quan, K. Schierle-Arndt, P. Yang, Nano Lett. 20 (2020) 3734–3739.
[7] L. Lian, M. Zheng, W. Zhang, L. Yin, X. Du, P. Zhang, X. Zhang, J. Gao, D. Zhang, L. Gao, G. Niu, H. Song, R. Chen, X. Lan, J. Tang, J. Zhang, Adv. Sci. 7 (2020) 2000195.
[8] S. Cheng, A. Beitlerova, R. Kucerkova, E. Mihokova, M. Nikl, Z. Zhou, G. Ren, Y. Wu, ACS Appl. Mater. Interfaces 13 (2021) 12198–12202.
[9] M. Zhang, X. Wang, B. Yang, J. Zhu, G. Niu, H. Wu, L. Yin, X. Du, M. Niu, Y. Ge, Q. Xie, Y. Yan, J. Tang, Adv. Funct. Mater. 31 (2020) 2007921.
[10] W. Zhu, R. Li, X. Liu, X. Xu, H. Chao, H. Wang, Y. Jiao, H. Liu, F. Xu, Z. Nie, Y. Gao, R. Wang, J. Zhu, W. Huang, Adv. Funct. Mater. 34 (2024) 2316449.
[11] B. Yang, L. Yin, G. Niu, J.-H. Yuan, K.-H. Xue, Z. Tan, X.-S. Miao, M. Niu, X. Du, H. Song, E. Lifshitz, J. Tang, Adv. Mater. 31 (2019) 19044711.
[12] Y. Wu, D. Han, B.C. Chakoumakos, H. Shi, S. Chen, M.-H. Du, I. Greeley, M. Loyd, D.J. Rutstrom, L. Stand, M. Koschan, C.L. Melcher, J. Mater. Chem. C 6 (2018) 6647–6655.
[13] H. Wu, Q. Wang, A. Zhang, G. Niu, M. Nikl, C. Ming, J. Zhu, Z. Zhou, Y.-Y. Sun, G. Nan, G. Ren, Y. Wu, J. Tang, Sci. Adv. 9 (2023) 1789.
[14] S. Cheng, A. Beitlerova, R. Kucerkova, M. Nikl, G. Ren, Y. Wu, Phys. Status Solidi Rapid Res. Lett. 14 (2020) 2000374.
[15] Q. Yao, J. Li, X. Li, X. Zheng, Z. Wang, X. Tao, Adv. Opt. Mater. 10 (2022) 2201161.
[16] T. Haposan, A. Arramel, P.Y.D. Maulida, S. Hartati, A.A. Afkauni, M.H. Mahyuddin, L. Zhang, D. Kowal, M.E. Witkowski, K.J. Drozdowski, M. Makowski, W. Drozdowski, L.J. Diguna, M.D. Birowosuto, J. Mater. Chem. C 12 (2024) 2398–2409.
[17] F. Gao, X. Zhu, Q. Feng, W. Zhong, W. Liu, H. Xu, Y. Liu, Nano Energy 98 (2022).
[18] Q. Xu, J. Wang, Q. Zhang, X. Ouyang, M. Ye, W. Xie, X. Yan, D. Li, X. Ouyang, X. Tang, X. Zhang, Photon. Res. (2021) 9.
[19] S. Cheng, M. Nikl, A. Beitlerova, R. Kucerkova, X. Du, G. Niu, Y. Jia, J. Tang, G. Ren, Y. Wu, Adv. Opt. Mater. 9 (2021).
[20] D. Yuan, ACS Appl. Mater. Interfaces 12 (2020) 38333–38340.
[21] S. Cheng, M. Nikl, A. Beitlerova, R. Kucerkova, X. Du, G. Niu, Y. Jia, J. Tang, G. Ren, Y. Wu, Adv. Opt. Mater. 9 (2021) 2100460.
[22] Q. Wang, Q. Zhou, M. Nikl, J. Xiao, R. Kucerkova, A. Beitlerova, V. Babin, P. Prusa, V. Linhart, J. Wang, X. Wen, G. Niu, J. Tang, G. Ren, Y. Wu, Adv. Opt. Mater. 10 (2022) 2200304.
[23] W. Chen, T. Wang, T. Wang, J. Yu, S. Yao, W. Feng, Q. Wang, L. Huang, X. Xu, X. Yu, Adv. Sci. 10 (2023) 2304957.
[24] Z. Wang, Y. Wei, C. Liu, Y. Liu, M. Hong, Laser Photon. Rev. 17 (2023) 2200851.
[25] L. Stand, D. Rutstrom, M. Koschan, M.-H. Du, C. Melcher, U. Shirwadkar, J. Glodo, E. Van Loef, K. Shah, M. Zhuravleva, Nucl. Instrum. Methods Phys. Res. Sect. A Accel. Spectrom. Detect. Assoc. Equip. 991 (2021) 164963.
[26] X. Li, J. Chen, D. Yang, X. Chen, D. Geng, L. Jiang, Y. Wu, C. Meng, H. Zeng, Nature Commun 12 (2021) 3879.
[27] Q. Wang, C. Wang, Z. Wang, X. Sun, M. Nikl, X. OuYang, Y. Wu, J. Phys. Chem. Lett. 13 (2022) 9066–9071.
[28] A.E. Borisevich, M.V. Korzhik, G.Y. Drobychev, J.F. Cavaignac, R. Chipaux, Nucl. Instrum. Methods Phys. Res. Sect. A Accel. Spectrom. Detect. Assoc. Equip. 537 (2005) 228–231.
[29] Y. Tratsiak, L. Stand, R. Lalk, M. Zhuravleva, C.L. Melcher, J. Lumin. 263 (2023) 119952.
[30] G. Liu, W. Chen, Z. Xiong, Y. Wang, S. Zhang, Z. Xia, Nat. Photonics 18 (2024) 562–568.
[31] B.-M. Liu, X.-X. Guo, L.-Y. Cao, L. Huang, R. Zou, Z. Zhou, J. Wang, Chem. Eng. J. 452 (2023) 139313.
[32] X. Dai, X. Zou, H. Zhang, W. Chen, C. Yang, M.S. Molokeev, Z. Xia, Y. Liu, X. Zhang, M. Zheng, B. Lei, Adv. Opt. Mater. (2023) 2302380.
[33] X. Wen, R. Kucerkova, V. Babin, P. Prusa, M. Kotykova, M. Nikl, W. Li, Q. Wang, S. Kurosawa, Y. Wu, J. Am. Ceram. Soc. 106 (2023) 6762–6768.
[34] X. Wen, P. Prusa, L. Vladimir, T. Parkman, V. Vanecek, D. Panek, M. Nikl, S. Cheng, Q. Wang, G. Ren, Y. Wu, ACS Appl. Electron. Mater. 6 (2023) 3507–3514.
[35] L. Redaelli, A. Mukhtarova, S. Valdueza-Felip, A. Ajay, C. Bougerol, C. Himwas, J. Faure-Vincent, C. Durand, J. Eymery, E. Monroy, Appl. Phys. Lett. 105 (2014).